SIAM J. NUMER. ANAL.
Vol. 35, No. 6, pp. 2370–2384, December 1998

013

SPECTRAL SIMULATION OF SUPERSONIC REACTIVE FLOWS*

WAI SUN DON† AND DAVID GOTTLIEB†

In memory of Ami Harten

Abstract. We present in this paper numerical simulations of reactive flows interacting with shock waves. We argue that spectral methods are suitable for these problems and review the recent developments in spectral methods that have made them a powerful numerical tool appropriate for long-term integrations of complicated flows, even in the presence of shock waves. A spectral code is described in detail, and the theory that leads to each of its components is explained. Results of interactions of hydrogen jets with shock waves are presented and analyzed, and comparisons with ENO finite difference schemes are carried out.

Key words. Chebyshev collocation, shock, Gibbs phenomenon, supersonic combustion

AMS subject classifications. 65P30, 77Axx

PII. S0036142997318966

1. Introduction.

In this paper we present numerical simulations of interactions of shock waves and smooth flows with complex structures. We show that properly designed spectral methods are especially suited for this type of problem since fine details of complex flow structures are required and long time integrations are involved.

We start by reviewing recent developments in the theory of spectral methods applied to time-dependent problems. In particular we review the Kosloff–Tal–Ezer transformation that enables us to use a reasonable time step while retaining spectral accuracy. Next, we discuss new developments in spectral methods for discontinuous solutions. The first is the complete resolution of the Gibbs phenomenon. This result demonstrates that the quality of spectral approximations to piecewise smooth functions is essentially the same as the approximations of smooth functions. The second development is spectral vanishing viscosity method. It has been shown that adding spectrally small viscosity to spectral codes leads to convergence to entropy-satisfying solutions. We suggest efficient ways to implement those methods by use of filtering.

The rest of the paper is devoted to the simulation of mixing enhancement by shock waves following the idea by Marble et al. [17]. The governing equations are the compressible reactive Navier–Stokes equations with multiple species undergoing multichemical reactions. We modeled the chemical reaction by a single step reversible reaction using four chemical species, H_2, O_2, H_2O, and N_2. We present results that were obtained only by spectral methods concerning fuel breakup. A comparison of mixing for different configurations is also presented. We conclude by presenting comparisons of timing for spectral and ENO schemes, using serial as well as parallel machines.

2. Spectral methods.

Most of the work reported in this paper has been carried out with the use of Chebyshev collocation methods.

A software library (PseudoPack) for computing derivatives based on Fourier, Chebyshev, and Legendre collocation methods can be obtained from

`http://www.cfm.brown.edu/people/wsdon/home.html`.

*Received by the editors March 26, 1997; accepted for publication September 5, 1997; published electronically November 13, 1998. This research was supported by grant 96-1-0150.
http://www.siam.org/journals/sinum/35-6/31896.html
†Division of Applied Mathematics, Brown University, Providence, RI 02912 (wsdon@hydra.cfm.brown.edu, dig@hydra.cfm.brown.edu).

For the time marching we use the low storage third-order TVD Runge–Kutta scheme of Shu and Osher [1] to solve the system of ODEs produced by the spatial differencing. It has the form

$$\begin{aligned} \vec{U}^1 &= \vec{U}^n + \Delta t L(\vec{U}^n), \\ \vec{U}^2 &= \frac{1}{4}(3\vec{U}^n + \vec{U}^1 + \Delta t L(\vec{U}^1)), \\ \vec{U}^{n+1} &= \frac{1}{3}(\vec{U}^n + 2\vec{U}^2 + 2\Delta t L(\vec{U}^2)). \end{aligned} \tag{2.1}$$

L is the spatial operator. $\vec{U}^n$and $\vec{U}^{n+1}$ are the data arrays at the nth and $(n+1)$th time step, respectively. $\vec{U}^1$and $\vec{U}^2$ are two temporary arrays at the intermediate Runge–Kutta stages. The scheme is stable for $\Delta t \approx O(N^{-2})$.

For smooth problems, this does not present an excessive burden since the required N for obtaining accurate solutions is small, typically in the range of $16 \sim 32$. For large N, however, the restrictive time step renders Chebyshev methods impractical for most real physical applications. For long time integration, excessive CPU time is needed to reach the final time.

To relax the $O(N^{-2})$ time-stepping restriction, we adopted the idea of a grid mapping technique as proposed by Kosloff and Tal-Ezer [2], namely,

$$x = g(\xi, \alpha) = \frac{\sin^{-1}(\alpha\xi)}{\sin^{-1}\alpha}, \tag{2.2}$$

where $\xi_j = \cos(\pi j/N), j = 0, \ldots, N$, are the original Chebyshev collocation points and x_j is a new set of interpolation points depending on the parameter $\alpha \in [0, 1]$.

It was shown in [2] that if α is chosen as

$$\alpha = \alpha(N, \epsilon) = \operatorname{sech}\left(\frac{|\ln \epsilon|}{N}\right), \tag{2.3}$$

then the approximation error is roughly ϵ. *By choosing ϵ to be machine zero, the error of the coordinate transformation is essentially guaranteed to be small.* Note that *α is not a constant but a function of N.*

If such a mapping is implemented, the Chebyshev collocation methods exhibit several highly desirable properties. We list two of the most relevant ones.

1. The reduction of roundoff error from $O(N^{2k}\epsilon)$ to $O(N^k\epsilon)$, where k is the order of differentiation [3].
2. The spectral radius of the differentiation matrix with mapping is asymptotically of $O(N)$ as opposed to $O(N^2)$ for the unmapped case.

The implementation of the mapping (2.2) along with the proper choice of α according to (2.3) changes the necessary condition for stability from $\Delta t \propto N^{-2}$ to $\Delta t \propto N^{-1}$.

3. Approximation theory. In spectral methods the approximation error depends only on the regularity of the approximated function. A typical error estimate is of the form

$$|f(x) - f_N(x)| \le C N^{\frac{1}{2}-p} \left(\int_0^{2\pi} |f^{(p)}(t)|^2 dt\right)^{\frac{1}{2}},$$

where $f_N(x)$ is the Fourier approximation to the function $f(x)$ and $f^{(p)}$ denotes the pth derivative of f.

Similar expressions hold for other spectral and pseudospectral approximations. The result shows that smoother functions yield better approximations, and the error depends on the pth derivative of the function. In fact, if the function is analytic then

$$|f(x) - f_N(x)| \leq Ce^{-\alpha N}\,,$$

resulting in exponential convergence.

A related result is that in order to resolve a wave using Chebyshev collocation (pseudospectral) methods one needs to use π points per wavelength [4] while $16 \sim 20$ points are needed for low-order finite difference schemes. Note that the theoretical limit is 2 points per wavelength.

The accuracy of spectral methods leads to codes that use a minimal number of grid points to obtain the same results obtained by lower-order methods with many more grid points. Alternatively, for limited resources, spectral methods serve as an ideal tool to gain deep insights into the physics by providing maximum resolution.

The question is whether these results hold for piecewise smooth functions. The folklore is that all the properties concerning the high accuracy are lost. One often hears quoted the *Gibbs phenomenon*.

In fact, the same accuracy obtained for smooth functions can be obtained for piecewise smooth functions. In a series of papers [5, 6, 7, 8, 9], it was shown that given the spectral approximation to a piecewise smooth function one can construct an exponentially convergent approximation to the function. This result had been proven for Fourier, Chebyshev, Legendre, and spectral methods based on spherical harmonics.

In the following we shall briefly review several methods to enhance the accuracy.

For the ease of presentation, we discuss the results for Fourier approximations, since nothing essential is lost in the Chebyshev case.

Given the Fourier approximation

$$f_N(x) = \sum_{k=-N}^{N} \hat{f}_k e^{i\pi kx},$$

we construct a filtered sum

$$f_N^\sigma(x) = \sum_{k=-N}^{N} \sigma\left(\frac{k}{N}\right) \hat{f}_k e^{i\pi kx}\,. \tag{3.1}$$

Following Vandeven [10] we define a $(p > 1)$-order filter function $\sigma(\omega)$ as a $C^\infty[-1,1]$ function satisfying

$$\begin{aligned} &\sigma(0) = 1\,, \qquad \sigma(\pm 1) = 0\,, \\ &\sigma^{(j)}(0) = 0\,, \quad \sigma^{(j)}(\pm 1) = 0\,, \qquad j \leq p \end{aligned} \tag{3.2}$$

where $\sigma^{(j)}$ denotes the jth derivative.

It can be shown that the filtered sum (3.1) approximates the original function very well away from the discontinuities. A good example of filter function is the exponential filter. It is defined as

$$\sigma(\omega) = \exp\left(-\alpha|\omega|^\beta\right)\,, \tag{3.3}$$

where $-1 \leq \omega = k/N \leq 1$, $k = -N, \ldots, N$, and $\alpha = -\ln\epsilon$, ϵ is the machine zero, and β is the order of the filter.

The exponential filter offers the flexibility of changing the order of the filter simply by specifying a different β. One does not have to write a different filter for different order. Thus varying β with N yields exponential accuracy according to [10].

The above-defined filters do not completely remove the Gibbs phenomenon as oscillations still exist in the neighborhood of the discontinuities. In order to recover the full accuracy in any region where the function is continuous, one must use a different idea. In [8] it is shown how to use a known set of $2N+1$ Fourier coefficients to obtain the coefficients of a different expansion (based on the Gegenbauer polynomials). The new expansion converges *exponentially* in any smooth region.

In practice, when solving differential equations one uses the exponential filter at every time step and the Gegenbauer filter at the end of the calculations as a postprocessor.

When spectral methods are applied to nonlinear hyperbolic equations in conservation form the problem of an entropy-satisfying solution arises. In fact, there is no artificial dissipation in the method to indicate that the solution is a limit of a dissipative process. One clearly needs to add artificial dissipation. However, this dissipation must be spectrally small in order not to affect the overall accuracy. This problem has been addressed in [11, 12, 13].

It has been shown that with a suitable addition of (spectrally small) artificial dissipation to the high modes only, the method converges. In this paper we used one version of the above idea: the super vanishing viscosity (SVV) method suggested by Tadmor [11, 12].

For the sake of illustration consider the nonlinear scalar hyperbolic equation

$$u_t + f(u)_x = 0.$$

A spectral approximation involves seeking a polynomial of degree N, $u_N(x,t)$, such that

$$\frac{\partial}{\partial t}u_N + \frac{\partial}{\partial x}f_N(u_N) = 0\,.$$

In the SVV method the equation is regularized by an additional term,

$$\frac{\partial}{\partial t}u_N + \frac{\partial}{\partial x}f_N(u_N) = \epsilon(-1)^{s+1}Q^{2s}u_N\,, \tag{3.4}$$

where $Q = \sqrt{1-x^2}\frac{\partial}{\partial x}$.

In [14] it was shown that if $\epsilon = \alpha N^{1-2s}$ where $s \sim \log N$, then (3.4) converges to the correct entropy solution.

It turns out that the SVV method can easily be applied if one uses the time-splitting technique and solves in the first step

$$\frac{\partial}{\partial t}u_N + \frac{\partial}{\partial x}f_N(u_N) = 0$$

and in the second step

$$\frac{\partial}{\partial t}u_N = \epsilon(-1)^{s+1}Q^{2s}u_N\,.$$

We note that the Chebyshev polynomials $T_k(x)$ are the eigenfunctions of the operator Q^2 with eigenvalues k^2. Thus if

$$u_N(x,t) = \sum_{k=0}^{N} a_k(t)T_k(x)\,,$$

then solving the second step analytically over one time step is equivalent to modifying the Chebyshev coefficients $a_k(t)$ as

$$a_k(t+\Delta t) = a_k(t)\exp(-\alpha N \Delta t (k/N)^{2s})\,.$$

This is a *low pass filter* that can be performed without any additional work.

4. Supersonic combustion. Recent advances in computing power and memory storage capacity sparked a renewed interest in computational modeling of complex problems in supersonic chemically reacting combustion systems. These systems might be used as advanced aerospace propulsion systems. One of the proposed systems is a hydrogen fuel supersonic combustion scramjet that is capable of propelling a vehicle at hypersonic speed in the atmosphere. For the current hypersonic vehicle configuration considered, the residence time the fuel spends in the engine to achieve maximum mixing with the supersonic air flow is limited to a few milliseconds. When increasing the Mach number in the combustor, the degree of fuel air mixing achieved through advection and diffusion processes is reduced, leading to an overall reduction of the combustion efficiency and thrust. However, some recent supersonic mixing layer experiments, both physical and numerical, indicate that the overall mixing process and the combustion efficiency can be improved by various techniques [15].

In a premixed combustion process, the combustion rate is limited by the rate at which reactants diffuse across the fuel-air interface. This diffusion rate is determined by the length of the interface and the concentration gradient across it. One way to increase this rate of diffusion is to stretch out the interface through the motion induced by a point vortex [16]. At the same time this would steepen the concentration gradient across the interface by bringing fresh reactants into contact with the fuel. Marble et al. [17] suggest a way to induce this vorticity by having a shock pass through a jet of fuel nearly perpendicular to its axis. While passing through the region of inhomogeneous density the shock will produce vorticity via the $\frac{\nabla\rho\times\nabla p}{\rho^2}$ term in the vorticity equation:

$$\frac{d\omega}{dt} = (\omega\cdot\nabla)V - \omega\nabla\cdot V + \frac{\nabla\rho\times\nabla p}{\rho^2}.$$

The gradient in pressure across the shock in conjunction with the gradient in fluid density between the air and hydrogen produce a large increase in vorticity as the shock passes through the hydrogen jet. This phenomenon was investigated by many researchers, e.g., [18, 17, 19, 20, 21] (see [22] for a full list of references). Their results demonstrate a similar vortical splitting and rollup. However, there are unexplained quantitative differences in features such as size, spacing, and velocity of the vortical structure. Each of these studies addresses only a limited range of flow conditions, and, they do not address the question of mixing.

In this paper, we apply spectral methods to this difficult problem. At this stage of research, we have developed a two-dimensional combustion code using the numerical techniques mentioned in the previous sections. A three-dimensional version of the algorithm is currently under development. The algorithm is described in detail in [22]. Here we shall refer the algorithm simply as the *spectral code*.

4.1. Navier–Stokes equations.

4.1.1. The physical model. The two-dimensional governing equations of combustion in Cartesian coordinates describe the conservation of mass, momentum, energy, and N_s chemical species undergoing multichemical reactions as

$$\mathbf{U}_t + \mathbf{F}_x + \mathbf{G}_y = \mathbf{V}_x + \mathbf{W}_y + \mathbf{C}\,. \tag{4.1}$$

The terms $\mathbf{F}$ and $\mathbf{G}$ are the inviscid fluxes. $\mathbf{V}$ and $\mathbf{W}$ contain the diffusive part of the problem and $\mathbf{C}$ is the chemical source term.

The state vector $\mathbf{U}$ is

$$\mathbf{U} = (\rho, \rho u, \rho v, \rho E, \rho\, \mathbf{f})^{\mathrm{T}} ,$$

where fluid density is ρ, $\mathbf{u} = (u, v)^{\mathrm{T}}$ is the fluid velocity, E is the specific total energy, and $\mathbf{f}$ is the vector of mass fractions $\mathbf{f} = (f_1, \ldots, f_{N_s-1})$ for $N_s - 1$ chemical species. The mass fraction of the last species f_{N_s} can be derived from the law of conservation of species,

$$\sum_{i=1}^{N_s} f_i = 1 .$$

Each species f_i drifts at a velocity $\tilde{\mathbf{u}} = (\tilde{u}_i, \tilde{v}_i)^{\mathrm{T}}$ relative to the mean mixture velocity $\mathbf{u}$.

In terms of these variables and the pressure P, the inviscid fluxes are given by

$$\mathbf{F} = (\rho u, \rho uu + P, \rho uv, (\rho E + P)u,\ (u + \tilde{u}_1)\rho f_1, \ldots, (u + \tilde{u}_{N_s-1})\rho f_{N_s-1})^{\mathrm{T}} ,$$
$$\mathbf{G} = (\rho v, \rho uv, \rho vv + P, (\rho E + P)v,\ (v + \tilde{v}_1)\rho f_1, \ldots, (v + \tilde{v}_{N_s-1})\rho f_{N_s-1})^{\mathrm{T}} .$$

The Stokes assumption implies that the elements of the viscous stress tensor take the form

$$\tau_{xx} = \frac{4}{3}u_x - \frac{2}{3}v_y, \quad \tau_{yy} = \frac{4}{3}v_y - \frac{2}{3}u_x, \quad \tau_{xy} = \tau_{yx} = u_y + v_x.$$

Thus the viscous terms become

$$\mathbf{V} = \mu\ (\tau_{xx}, \tau_{yx}, \sigma_1, 0, \ldots, 0)^{\mathrm{T}} ,$$
$$\mathbf{W} = \mu\ (\tau_{xy}, \tau_{yy}, \sigma_2, 0, \ldots, 0)^{\mathrm{T}} ,$$

where μ is the mixture viscosity.

A Prandtl number, $P_r = 0.72$, is used to relate the fluid viscosity and the thermal diffusion, and a Schmidt number, $S_c = 0.22$, relates the viscosity and the molecular diffusion. Thus, in terms of the temperature T and the mixture-specific heat at constant pressure $\bar{C}_p$ and the species-specific enthalpy h_i, we have

$$\tilde{\mathbf{u}} = \frac{\mu}{\rho S_c}\nabla\, \mathbf{f} ,$$

$$\sigma_1 = u\tau_{xx} + v\tau_{xy} + \frac{\bar{C}_p}{P_r}T_x - \frac{\rho}{\mu}\sum_{i=1}^{N_s} h_i \tilde{u}_i f_i ,$$

$$\sigma_2 = v\tau_{yy} + u\tau_{yx} + \frac{\bar{C}_p}{P_r}T_y - \frac{\rho}{\mu}\sum_{i=1}^{N_s} h_i \tilde{v}_i f_i .$$

The Soret and Dufour effect, heat radiant effect, pressure gradient diffusion, and body forces are neglected. The binary coefficient of all species is assumed to be equal and the Lewis number $Le = 1$.

4.1.2. Thermodynamic model. The high temperatures produced by combustion imply that the perfect gas equation of state is a reasonable approximation:

$$p = \rho \bar{R} T .$$

$\bar{R}$ is a mixture gas constant computed by weighting the perfect gas constant R by the appropriate average of the species molecular weights M_i:

$$\bar{R} = R\sum_{i=1}^{N_s} f_i/M_i\,.$$

The specific total internal energy is given by

$$E = \int_0^T \bar{C}_p(s)\,ds - \frac{p}{\rho} + \frac{u^2}{2} + \frac{v^2}{2} + \sum_{i=1}^{N_s} f_i h_i^0\,,$$

where h_i^0 is the reference enthalpy of species i and $\bar{C}_p$ is a mixture-specific heat at constant pressure computed from the individual species-specific heats C_{p_i} as

$$\bar{C}_p = \sum_{i=1}^{N_s} C_{p_i} f_i/M_i\,.$$

C_{p_i} is approximated by a fourth-order polynomial in temperature, and thus its integral may be obtained analytically.

The coefficients for this approximation were obtained from [23]. The specific enthalpy of species h_i may be obtained in a similar way as

$$h_i = h_i^0 + \int_0^T C_{p_i}(t)\,dt\,.$$

4.1.3. Diffusion models. Sutherland's law provides an individual species viscosity

$$\frac{\mu_i}{\mu_0} = \left(\frac{T}{T_0}\right)^{3/2}\left(\frac{T_0+S}{T+S}\right)\,,$$

where μ_0, T_0, and S are species-dependent constants and are tabulated by Svehla [24].

The mixture viscosity may then be obtained by the empirical model known as Wilke's law [25] as

$$\mu = \sum_{i=1}^{N_s} \frac{\mu_i X_i}{\sum_{j=1}^{N_s} X_j \phi_{ij}}\,,$$

where

$$\phi_{ij} = \frac{\left\{1 + [(\mu_i/\mu_j)(f_j/f_i)]^{\frac{1}{2}}\,(M_i/M_j)^{\frac{1}{4}}\right\}^2}{[8(1+(M_i/M_j))]^{\frac{1}{2}}}$$

and $X_i = f_i/M_i$ is the mole fraction of species i.

4.1.4. Chemical model. The chemical reaction is modeled by a single-step reversible reaction using four chemical species ($N_s = 4$) as

$$2\mathrm{H}_2 + \mathrm{O}_2 \rightleftharpoons 2\mathrm{H}_2\mathrm{O}\,. \tag{4.2}$$

The fourth species is the inert gas N_2.

A modified Arrhenius law gives the equilibrium reaction rate k_e, the forward reaction rate k_f, and the backward reaction rate k_b as

$$\begin{aligned} k_e &= A_e T \exp(4.60517(E_e/T - 2.915)), \\ k_f &= A_f \exp(-E_f/(R^0 T)), \\ k_b &= k_f/k_e, \end{aligned}$$

where R^0 is the universal gas constant, the activation energy $E_e = 12925, E_f = 7200$, and the frequency factor $A_e = 83.006156, A_f = 5.541 \times 10^{14}$.

If we identify the first species with H_2, the second species with O_2, the third species with H_2O, and the fourth species as N_2, then the law of mass action is used to find the net rate of change in concentration of species i $\dot{C}_i$ by the single reaction (4.2), i.e.,

$$\begin{aligned} \dot{C}_1 &= 2k_f[H_2]^2[O_2] - k_b[H_2O]^2, \\ \dot{C}_2 &= -k_f[H_2]^2[O_2] - k_b[H_2O]^2, \\ \dot{C}_3 &= 2k_f[H_2]^2[O_2] - k_b[H_2O]^2, \end{aligned}$$

where $[\cdot]$ denotes the net rate of change in concentration.

The chemical source term $\mathbf{C}$ becomes

$$\mathbf{C} = \left(0, 0, 0, 0, \dot{C}_1 M_1, \dot{C}_2 M_2, \dot{C}_3 M_3\right)^{\mathrm{T}} . \tag{4.3}$$

4.2. Conservation of species. The solution of system (4.1) satisfies the law of conservation of species,

$$\sum_{i=1}^{N_s} f_i = 1, \qquad f_i \geq 0,\ i = 0, \ldots, N_s\,. \tag{4.4}$$

However, during the computations (4.4) is not satisfied exactly. When low-order schemes are used it is very important to impose (4.4) at every time step.

Due to the local nature of the law of conservation of species, *explicit* implementation of the law often leads to instability for global methods such as spectral methods. Therefore, the law is enforced *implicitly* by the numerical scheme by evolving all N_s number of species equations together while $f_i \geq 0$, $i = 0, \ldots, N_s$, is not enforced at all. For smooth problems, the species should be conserved at the level of the truncation error of the numerical scheme. Hence, it is advantageous to use high-order (spectral) methods. For the supersonic reactive flow, the maximum conservative error of species after the shock passes the hydrogen cylinder is $O(10^{-5})$. The disadvantage of such an approach is that additional computational resources are required for solving the additional PDEs.

4.3. Numerical experiments. The spectral code is used to simulate a two-dimensional planar shock in air interacting with hydrogen cylinder jets in three different initial configurations. The left figure of Figure 4.1 shows the case of a single jet centered at (2.75 cm, 0 cm). The second figure shows two aligned jets centered at (2.75 cm, 0 cm) and (6.75 cm, 0 cm). In the third case the two non-aligned jets are centered at (2.75 cm, 1 cm) and (6.75 cm, −1 cm).

The temperature of the hydrogen and air in the undisturbed region ahead of the shock is set to 1000° K with a pressure of 1 atm and zero velocity. The radius of the hydrogen cylinder is 1 cm, and reflecting boundaries parallel to the x-axis are placed

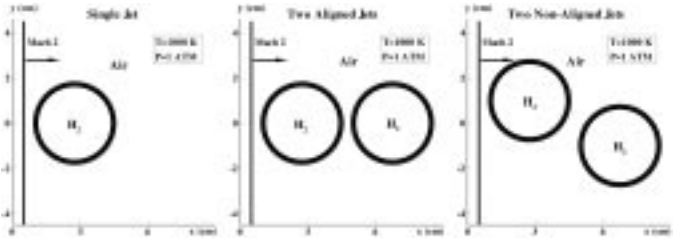

FIG. 4.1. *Initial density conditions of the supersonic combustion.*

6.5 cm above and below the axis of the cylinder. Supersonic inflow and characteristic outflow boundary conditions are imposed upstream and downstream, respectively, of a Mach 2 shock at $x_s = 0.5$ cm. The hydrogen cylinder has an initial diffused boundary given by the equation for its mass fraction in terms of the radius r,

$$f_i = \begin{cases} \exp(-\alpha(\frac{r}{r_0})^{16}), & r \le r_0, \\ 0 & \text{otherwise}, \end{cases} \qquad i \neq N_s, \quad \text{and} \quad f_{N_s} = 1 - \sum_{i=1}^{N_s - 1} f_i,$$

where $r_0 = 1$ cm and α is related to the logarithm of the numerical precision of floating point numbers. For these calculations, α is taken to be 32.66.

We ran the spectral code for these three cases up to 135μs or longer. In Figures 4.2, 4.3, and 4.4, we plot the contours of the density, H_2 and H_2O mass fraction at time 125μs for the cases of a single jet, two aligned jets, and two nonaligned jets, respectively.

4.3.1. Fuel breakup and mixing. An interesting new phenomenon that could also be responsible for enhancing fuel-air mixing (in addition to the idea of Marble et al.) was observed in this study. In Figure 4.5, a time sequence of the H_2O mass fraction at time 56μs, 58μs, 62μs and 68μs is shown. At time 56μs, a flame jet carrying oxygen penetrating into the hydrogen fuel can be seen. (We are using the case of two nonaligned jets as an example.) The heavier fluid (H_2O and O_2) is accelerated by the shock penetrating into the lighter fluid (H_2) and tends to form fingers (related to the Richtmyer–Meshkov instability [26]). A vortex (mushroom-shaped structure related to the Kevin–Helmholtz instability) forms at the tip of the flame jet. The flame jet cuts through the hydrogen fuel and makes contact with the air on the other side of the fuel-air interface at time 58μs. The vortex at the tip of the flame jet lifts and breaks up the fuel-air interface as depicted at time 62μs. At time 68μs, the motion of the vortex creates another flame jet allowing fresh air to penetrate inside and to interact with the fuel. This process repeats itself as the new flame jet reaches the other side of the fuel-air interface.

For low-order schemes, a similar phenomenon can be observed except that the large dissipation inherent in such schemes deters the formation of the mushroom structure (vortex) at the tip of the flame jet. Therefore, the low-order scheme predicts the large scale vortical rollup but not the break-up of the fuel.

Since the flow is driven mainly by the hyperbolic part of the PDE and the viscosity plays a minor role in these cases, one could imagine that the rollup of the vortices should exhibit layers of flame front. Such layers are clearly visible in the solution as computed by the spectral code (see Figure 4.2). Lower order schemes, with their substantial artificial viscosity, tend to smear the layers resulting in an unrealistic evolution of the flow field inside the fuel and the fuel-air mixing process.

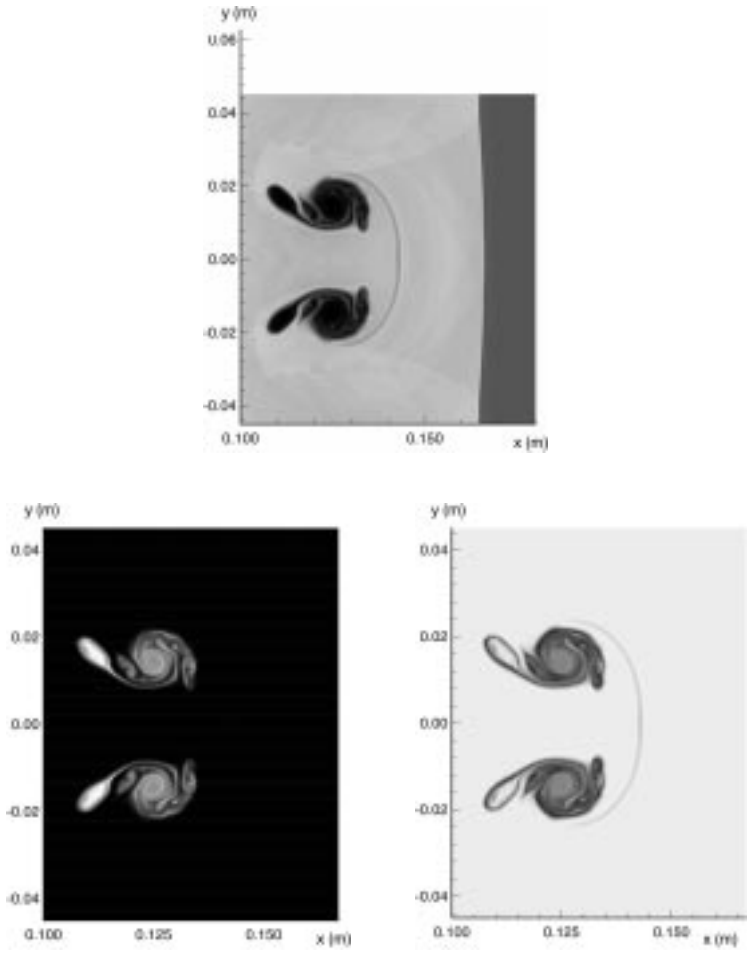

FIG. 4.2. *The density (top),* H_2 *(bottom left), and* H_2O *(bottom right) mass fractions for the single jet case at time* $t = 125\mu s$.

Hydrogen has a lower density than air, and therefore the local Mach number is much higher resulting in a higher shock speed. When coupled with the circular geometry of the hydrogen fuel, a circular curve shock appears far ahead of the rest of the shock (see Figure 4.3). Other complicated flow features such as triple Mach points, curved and reflected shocks, flame fronts, and break-up of the H_2 jets are also observed. The time evolution of the flow fields is the best way to appreciate the development of such flows. In Figures 4.3 and 4.4, the interaction of the two jets in different configurations yields a very rich and complicated scenario of coherent structures. As is evident from these two cases, the case of two aligned jets retains some form of large coherent structures while the case of two nonaligned jets breaks into many small pieces. In the case of two aligned jets, the fuel seems to mix pretty well with the air, but the large coherent structures lack the ability of drawing more fresh air from outside. Hence, the growth rate of the mixing efficiency will be slow. In the case of two nonaligned jets, the two jets break into many smaller fuel cells. The fuel-air interface was stretched by the vortical fluid motion, allowing better mixing of the fuel with fresh O_2. This observation is supported by computing the mixing efficiency for these three cases (Figure 4.6).

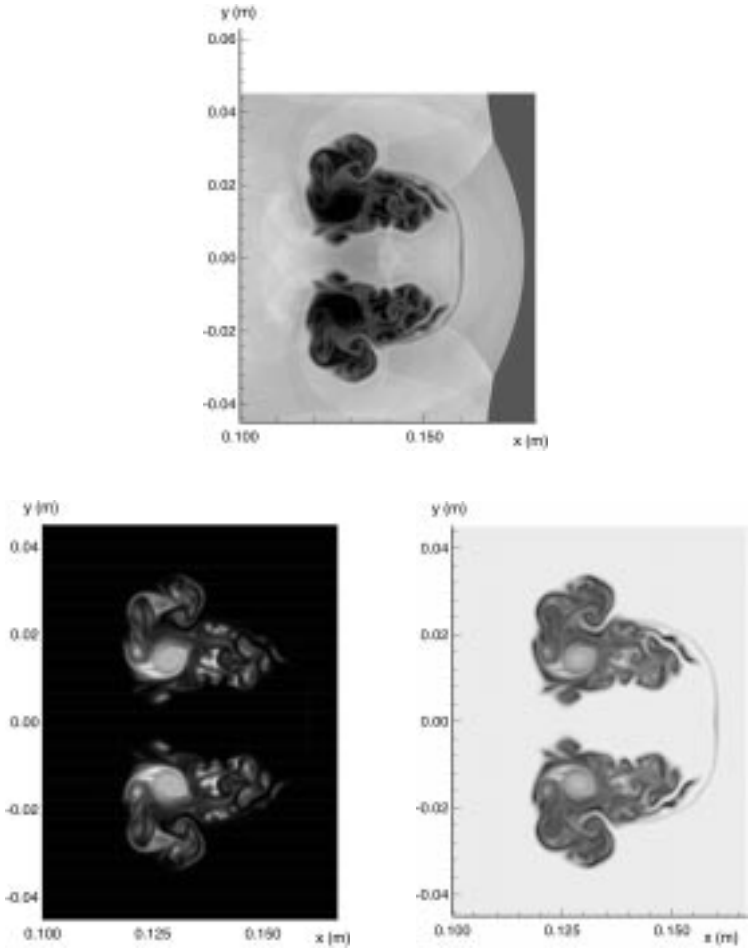

FIG. 4.3. *The density (top),* H_2 *(bottom left), and* H_2O *(bottom right) mass fractions for the two aligned jets case at time* $t = 125\mu$s.

We define the mixing efficiency as

$$\frac{\int_\Omega \min(g_{H_2}(\cdot,t), g_{O_2}(\cdot,t))d\Omega}{\int_\Omega \min(g_{H_2}(\cdot,0), g_{O_2}(\cdot,0))d\Omega}, \tag{4.5}$$

where

$$g_{H_2} = (\rho_{H_2} + \rho_{H_2O} M_{H_2}/M_{H_2O}),$$
$$g_{O_2} = (\rho_{O_2} + \rho_{H_2O} M_{O_2}/M_{H_2O}) * (0.126),$$

over the domain Ω. It measures the amount of mixing possible under the stoichiometric conditions.

The mixing efficiency starts out more or less the same for all three configurations, as expected. However, the two-jets cases start to take over the single jet case at around $t = 75\mu$s. Between the two-jets cases, the two jets aligned at $y = 0$ cm have better mixing efficiency than the nonaligned case. The nonaligned case is growing at a rate greater than the aligned case and it seems to be able eventually to overtake the aligned case at a later time. Due to the large computational cost required for long

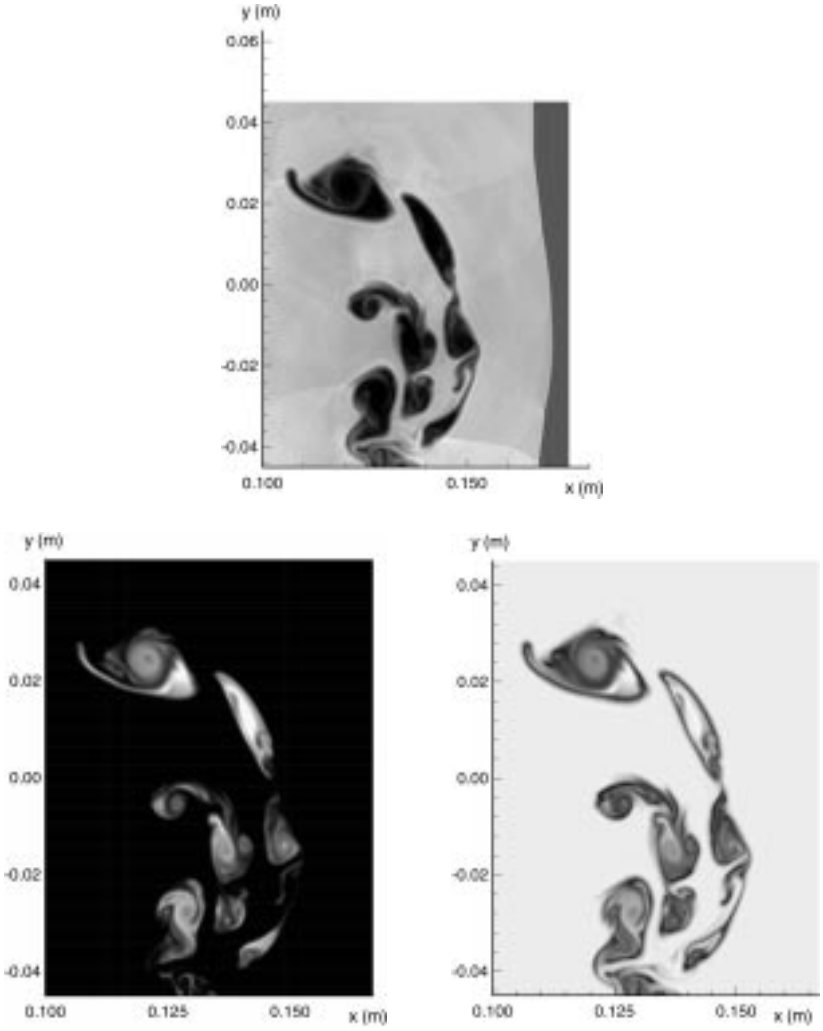

FIG. 4.4. *The density (top),* H_2 *(bottom left), and* H_2O *(bottom right) mass fractions for the two non-aligned jets case at time* $t = 125\mu$s.

time integration of the case of two nonaligned jets (smaller domain and no symmetry property can be exploited), the code was terminated at $t = 135\mu$s.

4.3.2. ENO versus spectral. For this type of problem, it is important to capture the complex physics with high accuracy. Using accurate calculations in search of quantitative information about the mixing requires high resolution and/or high-order schemes. Previous researchers failed to capture many important features of this flow due to the

- inability of their codes to adequately resolve features in the flow [18, 20, 21],
- inherently dissipative nature of the finite difference scheme, e.g., [20, 27]. Often, for long time integration, the loss of accuracy in earlier stages inhibits the development of fine scale features at later times.

In [22] we showed that the ENO results of the same simulations captured similar global structures as the spectral code but missed the time evolution of the small scale features.

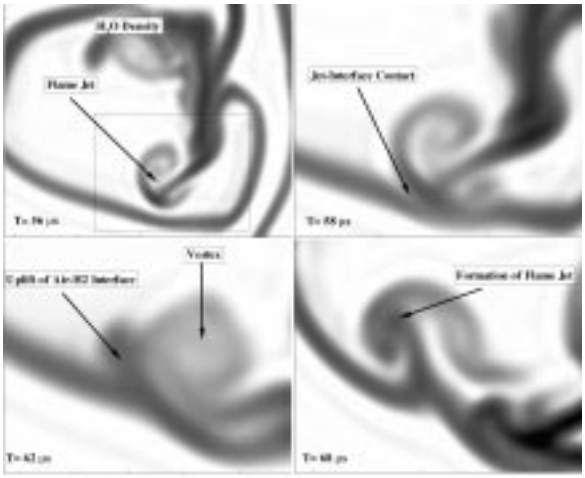

FIG. 4.5. *Time sequence plot of the flow mechanism that might also be responsible for enhancing fuel-air mixing at the time* $56, 58, 62$ *and* 68μs.

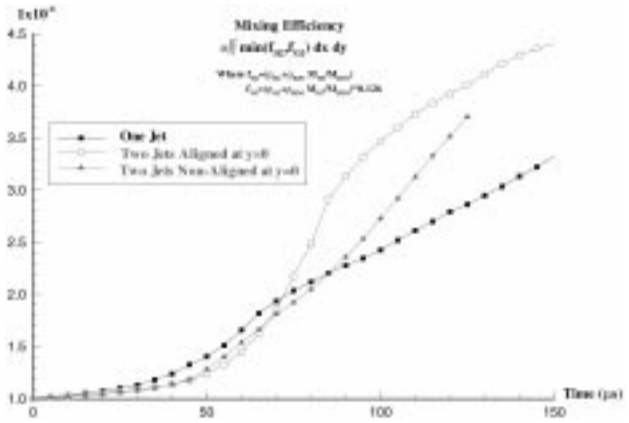

FIG. 4.6. *Mixing efficiency of three different jets' configurations.*

High-order schemes, e.g., fifth-order ENO schemes, provide more accurate solutions and resolve features better for a given grid. They are also computationally much more demanding than low-order schemes. However, for a given amount of CPU resources, they provide better-resolved results than lower-order versions, e.g., third-order ENO schemes. For these explicit schemes, the computational costs rise inversely as the third power of the grid point spacing. Spectral methods, on the other hand, resolve better both the large- and small-scale structures for long time integration, and do this at much lower computational cost. For example, for the grid size of $(512\times512/2)$, the CPU time for the spectral code is 4562 seconds on the single Cray C90 processor, while a third-order ENO scheme requires 8470 seconds on the CM5 with 32 nodes.

5. Parallel computing on the SP2. The two-dimensional combustion spectral code is written for both vector machine Cray C90 at CEWES HPC Center and IBM 24 Power2 Thin Nodes 2 Scalable Parallel System (SP2) using message passing

TABLE 5.1

CPU time (seconds) spent in each Runge–Kutta step for the reactive flow using Chebyshev Collocation methods (symmetric case). NP = number of SP2 Power2 Thin Nodes 2 processors.

NP/(N,M)	SP2			
	(256,256/2)	(512,512/2)	(1024,512/2)	(1024,1024/2)
1	6.9	N/A	N/A	N/A
2	7.0	29.0	N/A	N/A
4	4.5	22.5	58.0	N/A
8	1.6	11.1	40.0	86.0
16	1.7	4.4	8.1	28.0
20	1.9	4.1	7.7	13.0
	C90			
1	0.9	3.4	6.9	14.1

interface (MPI) communication protocol in the Center of Fluid Mechanics, Brown University. The specification of the SP2 can be found at

`http://www.cfm.brown.edu/tutorials/sp2.tutorial.html` .

The global nature of collocation methods presents a unique challenge for parallel computers with distributed memory architecture. In the single instruction multiple data (SIMD) scheme, slices of data are distributed to each processor's local memory, and each processor executes the same instructions. Interprocessor communications are initiated only if data needed for computation are located in other processors.

Finite difference schemes require communications only among a few nearby processors to obtain all the necessary pieces of data. In contrast, spectral methods (in one domain) require global communication of $O(N^2)$ (N being the number of grid points) to compute the differentiation of data across the processors.

In the current implementation, the data arrays are distributed in blocks of columns over each processor. We used the fast cosine transform algorithm (FCT) in the IBM Engineering and Scientific Subroutine Library (ESSL) to compute derivatives of data local in each processor. For derivatives of data distributed across different processors, a global transpose subroutine (PTRAN) using the the parallel version of ESSL was called before using the FCT algorithm. Since FCT requires that number of grid points N be odd and PTRAN demands that N be divisible by the number of processors, a pre-/post- processing step is needed to reorganize data into proper structures.

During each Runge–Kutta stage, this global transpose procedure must be called whenever differentiation is requested on data distributed across the processors. While the computations can be done efficiently on data local in each processor in $O(100)$ MFLOPS, the communication speed is only $O(10)$ MBytes/second. Depending on the grid size and number of processors, the range of the computation-to-communication ratio is only between 10% and 30%. In order to improve the efficiency of the parallel algorithm, we are studying different algorithms that would minimize the communication time.

In Table 5.1, we listed the timing of the computational kernel of the two dimensional combustion code for various grid dimensions versus the number of SP2 processors and a single Cray C90 processor. The timing is for the symmetric case in the y direction.

It can be seen that for sufficiently large problems $(N, M) > (512, 512/2)$ and 20 SP2 processors, the SP2 becomes as competitive as the single Cray C90 processor.

REFERENCES

[1] C. W. Shu and S. Osher, *Efficient implementation of essentially nonoscillatory shock-capturing schemes*, II, J. Comput. Phys., 83 (1989), pp. 32–78.

[2] D. Kosloff and H. Tal-Ezer, *Modified Chebyshev pseudospectral methods with $O(N^{-1})$ time step restriction*, J. Comput. Phys., 104 (1993), pp. 457–469.

[3] W. S. Don and A. Solomonoff, *Accuracy enhancement for higher derivatives using Chebyshev collocation and a mapping technique*, SIAM J. Sci. Comput., 18 (1997), pp. 1040–1055.

[4] D. Gottlieb and S. A. Orszag, *Numerical Analysis of Spectral Methods: Theory and Applications*, CBMS-NSF Regional Conf. Ser. in Appl. Math. 26, SIAM, Philadelphia, 1977.

[5] D. Gottlieb, C. W. Shu, A. Solomonoff, and H. Vandeven, *On the Gibbs phenomenon* I: *Recovering exponential accuracy from the Fourier partial sum of a nonperiodic analytic function*, J. Comput. Appl. Math., 43 (1992), pp. 81–98.

[6] D. Gottlieb and C. W. Shu, *Resolution properties of the Fourier method for discontinuous waves*, Comput. Meth. Appl. Mech. and Engrg., 116 (1994), pp. 27–37.

[7] D. Gottlieb and C. W. Shu, *On the Gibbs phenomenon* III: *Recovering exponential accuracy in a subinterval from a spectral partial sum of a piecewise analytic function*, SIAM J. Numer. Anal., 33 (1996), pp. 280–290.

[8] D. Gottlieb and C. W. Shu, *On the Gibbs phenomenon* IV: *Recovering exponential accuracy in a subinterval from a Gegenbauer partial sum of a piecewise analytic function*, Math. Comp., 64 (1995), pp. 1081–1095.

[9] D. Gottlieb and C. W. Shu, *On the Gibbs phenomenon* V: *Recovering exponential accuracy from collocation point values of a piecewise analytic function*, Numer. Math., 71 (1995), pp. 511–526.

[10] H. Vandeven, *Family of spectral filters for discontinuous problems*, J. Sci. Comput., 24 (1992), pp. 37–49.

[11] E. Tadmor, *Convergence of spectral methods for nonlinear conservation laws*, SIAM J. Numer. Math., 26 (1989), pp. 30–44.

[12] E. Tadmor, *Shock capturing by the spectral viscosity method*, in Proc. ICOSAHOM 89, Elsevier, North Holland, Amsterdam, 1989.

[13] Y. Maday, S. Ould Kaber, and E. Tadmor, *Legendre pseudospectral viscosity method for nonlinear conservation laws*, SIAM J. Numer. Anal., 30 (1993), pp. 321–342.

[14] H. Ma, *Chebyshev-Legendre super spectral viscosity method for nonlinear conservation laws*, SIAM J. Numer. Anal., 35 (1998), pp. 893–908.

[15] J. P. Drummond and H. S. Mukunda, *A Numerical Study of Mixing Enhancement in Supersonic Reaction Flow Fields*, AIAA Paper 88-3260, 1988.

[16] F. E. Marble, *Growth of a diffusion flame in the Field of a vortex*, in Recent Advances in the Aerospace Sciences, Corrado Casci, ed., Plenum Press, New York, 1985, pp. 395–412.

[17] F. E. Marble, E. E. Zukoski, J. W. Jacobs, G. J. Hendricks, and I. A. Waitz, *Shock Enhancement and Control of Hypersonic Mixing and Combustion*, AIAA Paper 90-1981, 1990.

[18] J. M. Picone and J. P. Boris, *Vorticity generation by shock propagation through bubbles in a gas*, J. Fluid Mech., 189 (1988), pp. 23–51.

[19] J. J. Quirk and S. Karni, *On the dynamics of a shock-bubble interaction*, J. Fluid Mech., submitted.

[20] J. Yang, T. Kubota, and E. E. Zukoski, *A model for characterization of a vortex pair formed by shock passage over a light gas inhomogeneity*, J. Fluid Mech., 258 (1994), pp. 217–244.

[21] V. T. Ton, *A Numerical Method for Mixing/Chemically Reacting Compressible Flow with Finite Rate Chemistry*, Ph.D. thesis, UCLA, 1993.

[22] W. S. Don and C. Quillen, *Numerical simulation of reactive flow, Part* I: *Resolution*, J. Comput. Phys., 122 (1995), pp. 244–265.

[23] B. J. McBride, S. Heimel, J. G. Ehlers, and S. Gordon, *Thermodynamic Properties to* 6000°*K for* 210 *Substances Involving the First* 18 *Elements*, NASA SP-3001, 1963.

[24] R. A. Svehla, *Estimated Viscosities and Thermal Conductivities of Gases at High Temperatures*, NASA report TR R-132, 1962.

[25] C. R. Wilke, *A viscosity equation for gas mixtures*, Chem. Phys., 18 (1950), pp. 517–519.

[26] E. E. Meshkov, *Instability of the interface of two gases accelerated by a shock wave*, Izv. Akad. Nauk. SSSR Mekh. Zhidk. Gaza, 4 (1969), pp. 101–104.

[27] J. P. Boris and D. L. Book, *Flux-corrected transport* I: *SHASTA—A fluid transport algorithm that works*, J. Comput. Phys., 11 (1973), pp. 38–69.